applied sciences

MDPI

Article

Development and Application of a New Reduction Coefficient of Water Pressure on Sub-Sea Tunnel Lining

Jinpeng Zhao [1,2,*], Zhongsheng Tan [1,2] and Ning Ma [1,2]

1 Key Laboratory for Urban Underground Engineering of Ministry of Education, Beijing Jiao Tong University, Beijing 100044, China; zhshtan@bjtu.edu.cn (Z.T.); 19125875@bjtu.edu.cn (N.M.)
2 School of Civil Engineering, Beijing Jiao Tong University, Beijing 100044, China
* Correspondence: 18115060@bjtu.edu.cn; Tel.: +86-188-1305-8046

Abstract: Limited drainage tunnels face pore water pressure, water inflow, and permeability challenges. At present, there is little systematic analysis and research on the lining water pressure of sub-sea tunnels, and there is a lack of verification of relevant engineering examples and field monitoring data. Based on the numerical simulation method, this paper discusses the lining water pressure and its reduction coefficient of the horseshoe section tunnel, which is verified by an engineering example. Based on many numerical simulations, the recommended value of the water pressure reduction coefficient considering the thickness of the grouting ring and grouting effect is put forward. The stress law and safety of tunnel lining under different water reduction coefficients are studied, and the safety of lining is evaluated combined with the measured data of lining stress. The results show that the numerical simulation has been well verified. Considering the water pressure according to the water pressure reduction coefficient method proposed in this paper can ensure the structural safety of tunnel lining. The method of lining water pressure reduction coefficient proposed in this paper can provide a reference for the subsequent lining design of the sub-sea tunnel.

Keywords: sub-sea tunnel; water pressure on lining; reduction coefficient; numerical simulation; field testing

Citation: Zhao, J.; Tan, Z.; Ma, N. Development and Application of a New Reduction Coefficient of Water Pressure on Sub-Sea Tunnel Lining. *Appl. Sci.* **2022**, *12*, 2496. https://doi.org/10.3390/app12052496

Academic Editors: Dajun Yuan, Dalong Jin and Xiang Shen

Received: 7 February 2022
Accepted: 25 February 2022
Published: 27 February 2022

1. Introduction

With the improvement of China's synthetic national power and the development of transportation, the construction of underwater tunnels has ushered in a good development period [1]. Unlike ordinary tunnels, underwater tunnels are always under the water body with an infinite water supply and constant water head during construction and operation. Thus, water pressure is one of the main loads in designing underwater tunnel lining structures. The determination of water pressure has always been a difficult and research hotspot in the structural design of underwater tunnel lining [2–4].

Many underwater tunnels, including sub-sea and mountain tunnels, have been built in the past century because of their convenience and economic benefits [5,6]. Considering the engineering geology and construction conditions [7], most underwater tunnels' waterproof and drainage design is fully closed or limited drainage. For fully closed tunnels, the lining shall withstand water pressure and earth pressure. However, tunnels with limited drainage face pore water pressure, water inflow and permeability [8,9]. Therefore, many scholars try to establish reliable methods to estimate the tunnel water pressure and seepage field distribution. This research topic usually adopts two methods, namely, the analytical method and the numerical method [10–13].

Early researchers, such as Bouvard and Pinto [14], provided approximate solutions for estimating the effective stress caused by water pressure and seepage around the tunnels. Fernandez and Alvarez [15] and Lei [16] established a flow network by using the mirror image method proposed by Harr [17] and obtained the excess pore pressure of the two-dimensional elastic problem entering the porous elastic rock mass from the tunnels. Joo and

Shin [18] determined the relationship between water pressure and the inflow rate of laminar and turbulent flow in underwater tunnels. El Tani [19] and Kolymbas and Wagner [20] adopted another analytical method, conformal mapping, to study this problem under different boundary conditions along the tunnels, such as zero water pressure and constant water head. Huangfu et al. [21] verified this method with the FLAC3D software. Wang et al. [22] proposed a simple model to calculate the lining water pressure with controlled drainage.

Previous studies are mainly limited to theoretical analysis, numerical simulation, and model test methods, and most studies mainly focus on the analysis of the seepage field. There is a lack of systematic analysis of the external water pressure of tunnel lining and the verification of relevant engineering examples and field monitoring data. Therefore, based on the sub-sea tunnel project of Qingdao Metro Line 8, through the combination of numerical calculation and field test, combined with the actual situation of the project, the factors with significant influence effect are selected, and a selection table of underwater tunnel water pressure reduction coefficients considering these factors is proposed. The stress and safety of lining under different water pressure reduction degrees are studied, and the safety of tunnel lining is evaluated combined with field monitoring data.

2. Discussion on Water Pressure Reduction Coefficient of Sub-Sea Tunnel Lining

2.1. Numerical Analysis of External Water Pressure of Initial Support of Sub-Sea Tunnel

The F5 structural fracture zone section of the sub-sea tunnel in the Daqing section of Qingdao Metro Line 8 is the engineering background, based on the numerical calculation model, and according to the stratum and support structure design of this section, the external water pressure of sub-sea tunnel lining is calculated. This section is located in the slightly weathered to moderately weathered tuff stratum with joint development and the permeability coefficient of surrounding rock k_r = 0.6 m/d. The thickness of the grouting ring t_2 = 5 m and the permeability coefficient is considered as slightly weathered tuff, taking k_g = 0.01 m/d. The initial support is 0.3 m thick C25 shotcrete, the impermeability grade is P6 [23], and its permeability coefficient $k_i = 1.0 \times 10^{-8}$ m/d. The calculation results of external water pressure of model initial support are shown in Figure 1, and the water pressure at the marked position in the figure is shown in Table 1.

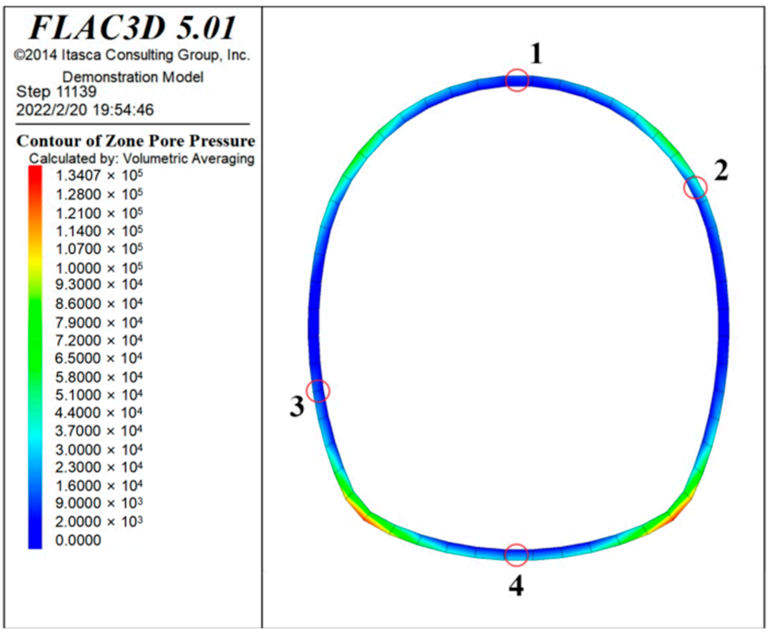

Figure 1. The external water pressure of initial support of the sub-sea tunnel (unit: Pa).

Table 1. The calculation results of initial support external water pressure.

Monitoring Points	1	2	3	4
Water pressure/kPa	11.53	12.66	18.74	31.54

It can be seen from Figure 1 and Table 1 that under the condition of water blocking and drainage restriction, the external water pressure distribution of the initial support is uneven, and the maximum water pressure is 134 kPa. The total head at the vault of the tunnel is 52 m, and the water pressure at each part is less than 30% of the total head. It shows that the water pressure outside the tunnel lining is not hydrostatic pressure. The water pressure is different at different positions. The water pressures of monitoring points 1–4 are 11.53, 12.66, 18.74, and 31.54 kPa, respectively.

2.2. Field Test on External Water Pressure of Initial Support of the Sub-Sea Tunnel

In order to verify the previous research on the external water pressure of the initial support of the sub-sea tunnel, the real-time on-site detection of the external water pressure of the initial support was carried out in the sea area of the Daqing section of Qingdao Metro Line 8. At the same time, to guide the construction, the monitoring sections are selected in the important and difficult construction section of the F5 structural fracture zone. A total of three monitoring sections are selected (see Figure 2). In Figure 2, F5 (red line) is an active fault, and the regional scope (ZDK41+990–ZDK42+200) is the area affected by the F5 fault. The surrounding rock in this area is broken under the influence of the F5 fault. The surrounding rock is grade IV–V, all of which are soft and broken surrounding rock. The classification of surrounding rock in Table 2 refers to the Chinese tunnel design code [23]. The total head height of the tunnel vault is 51–55 m. Pre-grouting water blocking measures are taken for all three sections. The statistics of the monitoring sections are shown in Table 2. The physical and mechanical parameters of the surrounding rock are shown in Table 3.

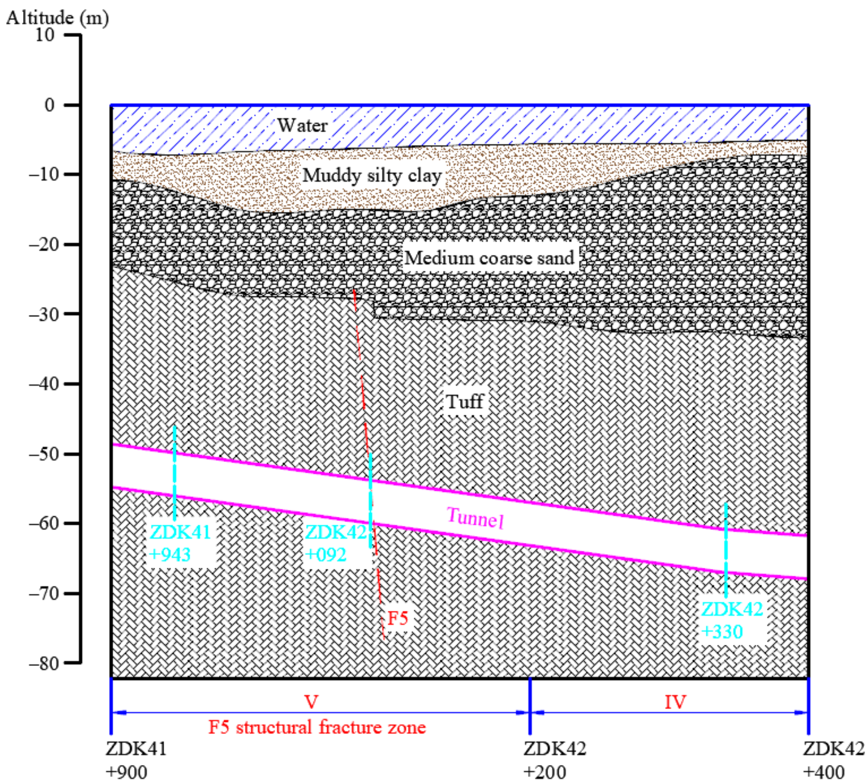

Figure 2. Local geological profile near the tunnel monitoring section.

Table 2. The statistics of monitoring sections.

Serial Number	Chainage	Waterhead	Surrounding Rock Grade	Waterproof and Drainage Scheme
1	ZDK41+943	54.2 m	IV	Controlled drainage
2	ZDK42+092	53.4 m	V	Controlled drainage
3	ZDK42+330	51.8 m	IV	Controlled drainage

Table 3. Physical and mechanical parameters of surrounding rock.

Materials	Density (kg/m^3)	Elastic Modulus (GPa)	Poisson's Ratio	Cohesion (kPa)	Internal Friction Angle (°)
Muddy silty clay	18.3	0.5	0.38	18.2	22.2
Medium coarse sand	20.1	0.8	0.28	20.2	35.3
Tuff	23.2	2.0	0.25	200.0	36.1

Six pore water pressure measuring points are arranged outside the initial support of each section. The layout of measuring points and the embedding position of instruments are shown in Figure 3. The vibrating wire pore water pressure sensor is selected as the instrument. The instruments and on-site installation photos are shown in Figure 4. After nearly five months of continuous monitoring, the time history curve of initial support external water pressure is obtained, as shown in Figure 5.

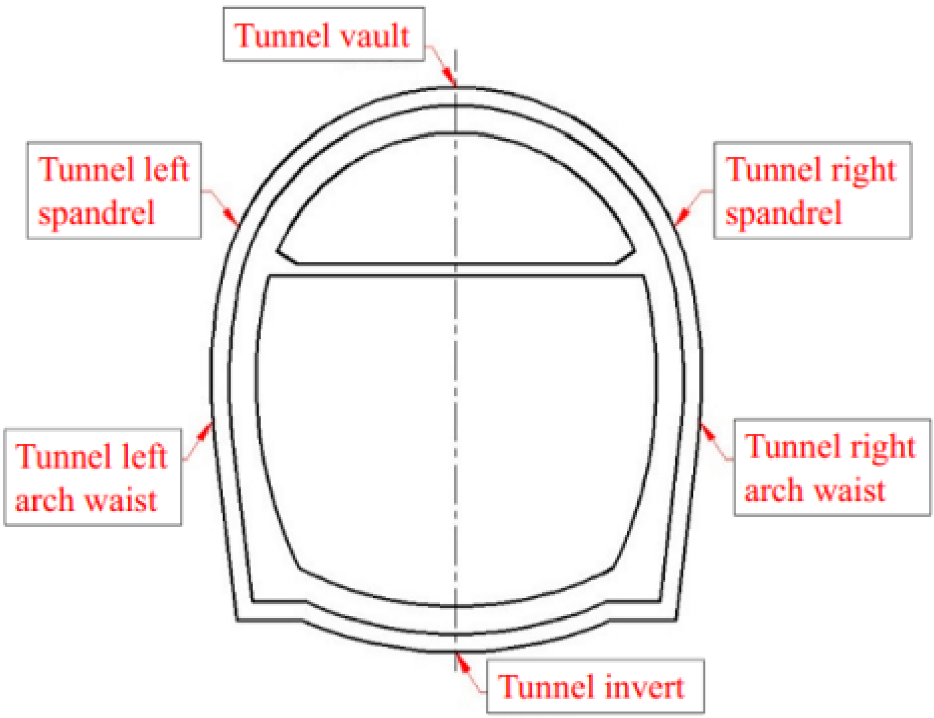

Figure 3. The external water pressure measuring points of initial support.

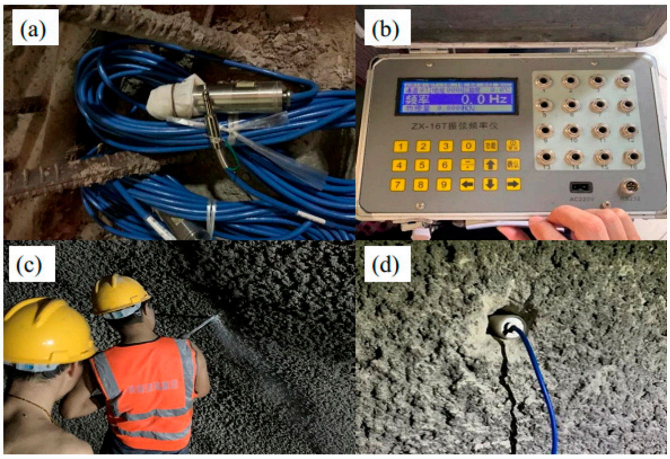

Figure 4. The pore water pressure sensor and field installation drawing: (**a**) pore water pressure sensor; (**b**) data acquisition instrument; (**c**) drill hole; (**d**) layout of the pore water pressure sensor.

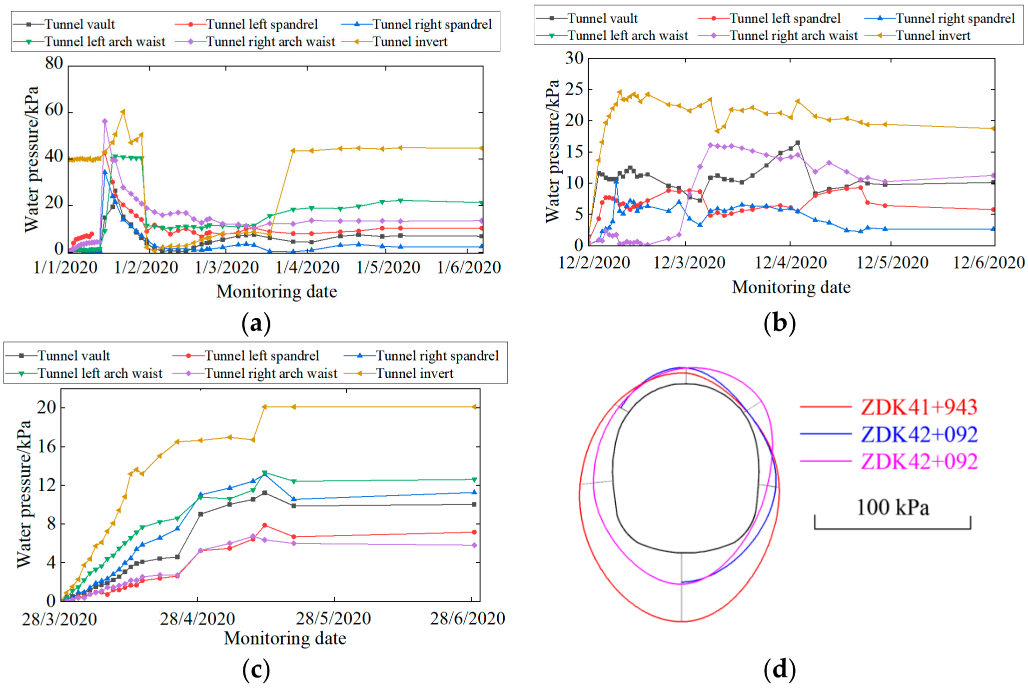

Figure 5. The initial support external water pressure: (**a**) the time-history curve of water pressure of the monitoring section ZDK41+943; (**b**) the time-history curve of water pressure of the monitoring section ZDK42+092; (**c**) the time-history curve of water pressure of the monitoring section ZDK42+330; (**d**) the water pressure distribution along the section. (The dates are in the form of "in the form of "day/month".)

It can be seen from Figure 5 that the external water pressure of the initial support of ZDK42+330 quickly is located in an F5 fracture zone. There was strong volatility in the early stage, although the external water pressure on the initial support of the two sections gradually stabilized after more than two months. ZDK41+943 and ZDK42+092 are located in the F5 bedrock fracture zone, although the two sections finally reach a stable state. However, there was strong volatility in the early stage, which gradually stabilized after two months. On the 14th day of monitoring, the external water pressure of the initial support of ZDK41+943 increased as a whole. The maximum value appears in the inverted arch, reaching 61 kPa, about 11% of the total head. After the water pressure of each part is maintained for about 1 week, it gradually drops to the normal level. Combined with the on-site construction, it is found that the reason is the poor drainage in this area. After the external water pressure of the lining is stable, the water pressure at the inverted arch is the largest. The water pressure at the tunnel invert for ZDK 41+943 and ZDK 42+092 is about twice the one at the other parts of the tunnel. The initial support water pressure of the three monitoring sections finally stabilized below 50 kPa, which is equivalent to the hydrostatic pressure generated by a 5 m water head. The total water head at the vault of the three sections of the tunnel is between 51 m and 55 m. It can be seen that the external water pressure of the initial support measured on site is less than 10% of the total water head.

2.3. Discussion on Reduction Coefficient of External Water Pressure of Initial Support of the Sub-Sea Tunnel

In order to analyze the difference between the numerical calculation results and the field measured results, the comparison is shown in Figure 6.

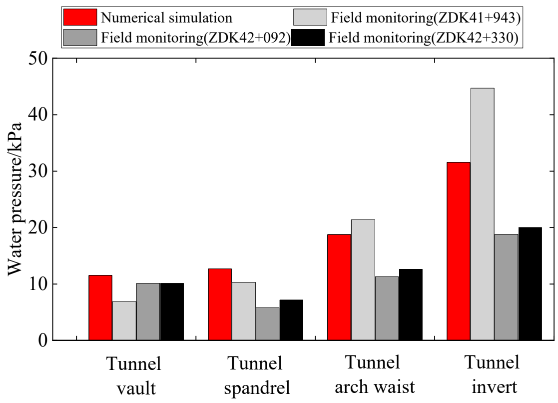

Figure 6. The comparison diagram of external water pressure of initial support of the sub-sea tunnel.

It can be seen from Figure 6 that the numerical calculation is slightly different from the field measurement of the external water pressure distribution of the initial support. Because the stratum is regarded as isotropic in the numerical calculation, and it is considered that the groundwater seeps evenly from the initial support surface, these factors lead to the difference in water pressure distribution. In addition, when installing the hydraulic force measuring sensor, after it is put into the borehole, it shall be sealed and fixed with fine sand and cement mortar. The cement mortar may affect the seepage path in front of the sensor. There is no big gap in the overall values, and this numerical model has strong applicability in this area.

2.4. Proposal of Water Pressure Reduction Coefficient

This paper puts forward the selection method of water pressure reduction coefficient of sub-sea tunnel lining, mainly considering three factors: surrounding rock permeability coefficient k_r, tunnel grouting ring thickness t_2 and grouting effect k_r/k_g. According to the permeability coefficient, the surrounding rock is divided into class A surrounding rock ($k_r \leq 0.2$ m/d), class B surrounding rock (0.2 m/d < $k_r \leq 0.8$ m/d), and class C surrounding rock (0.8 m/d < $k_r \leq 1$ m/d). The water pressure reduction coefficient selection under various surrounding rock conditions is shown in Tables 4–6. It should be noted that these reduction coefficients can only be used for horseshoe tunnels and have previously defined tunnel support thickness and permeability, and water level values. In addition, the recommended values in the following tables are based on the above discussion and a large number of numerical calculations. The water pressure reduction coefficients are directly given here, which is only a recommended value. Although a few reduction coefficients are verified above, more importantly, more similar projects need to be verified in the future.

Table 4. Recommended value of water pressure reduction coefficient of class A surrounding rock.

t_2 (m) \ k_r/k_g	5	10	50	100	200
1	0.95	0.90	0.75	0.65	0.60
3	0.95	0.60	0.25	0.20	0.15
5	0.95	0.50	0.16	0.15	0.10
7	0.90	0.45	0.15	0.15	0.10

Table 5. Recommended value of water pressure reduction coefficient of class B surrounding rock.

t_2 (m) \ k_r/k_g	5	10	50	100	200
1	1.00	0.95	0.80	0.70	0.65
3	1.00	0.70	0.30	0.25	0.20
5	0.95	0.60	0.25	0.20	0.15
7	0.95	0.55	0.20	0.20	0.10

Table 6. Recommended value of water pressure reduction coefficient of class C surrounding rock.

t_2 (m) \ k_r/k_g	5	10	50	100	200
1	1.00	0.95	0.85	0.75	0.70
3	1.00	0.80	0.35	0.30	0.25
5	1.00	0.65	0.30	0.25	0.20
7	0.95	0.60	0.25	0.20	0.15

2.5. Bearing Capacity of Secondary Lining under Different Water Pressure Reduction Coefficients

Based on the above research results, it is inferred that the initial support can form a closed structure with strong impermeability, which can bear large water pressure, while the water pressure on the secondary lining is very small. However, the long-term erosion of primary support shotcrete by seawater may seriously decline its impermeability and cannot play a good role in water plugging [24,25], which may increase the water pressure of the secondary lining. The initial support is shotcrete and includes steel arch, reinforcement mesh, and other structures, which is easy to produce weak sealing parts and even form cavities in them [26]. As the last line of defense of the tunnels, the secondary lining needs to consider the above situations in the design and must have high impermeability and bearing capacity as a safety reserve.

When calculating the bearing capacity of the lining structure, in order to ensure the safety of the tunnel lining structure, this paper assumes that the initial support is not waterproof. Considering that all the external water pressure of the initial support studied above acts on the secondary lining, the internal force of the lining structure is calculated, and then the reinforcement and safety factors are calculated. The calculation is mainly based on Code for Design of Metro [27] and Code for Design of Railway Tunnel [23].

This part of the calculation still takes the F5 fracture zone in the Daqing section of Qingdao Metro Line 8 as the engineering background and selects the representative class V surrounding rock section ZDK42+092 section to establish the model. Due to the influence of the fracture zone, the fractured rock at this section is extremely developed. The whole stratum is in loose to columnar structure, the surrounding rock is mainly jointed tuff, and the groundwater is bedrock fissure water. The total water head at the vault of the tunnel is 53.4 m. The secondary lining of section ZDK42+092 is 45 cm thick with C50 reinforced concrete structure. The physical and mechanical parameters of surrounding rock and concrete are shown in Table 7 [23], and the structural dimensions of the lining are shown in Figure 7.

Table 7. The physical and mechanical parameters of surrounding rock and concrete.

Materials	Density (kg/m^3)	Elastic Modulus (GPa)	Poisson's Ratio	Elastic Foundation Coefficient (MPa/m)	Coefficient of Earth Pressure at Rest
Surrounding rock (Tuff)	23.2	2.0	0.25	200	0.3
C50 concrete	25.0	35.5	0.20	—	—

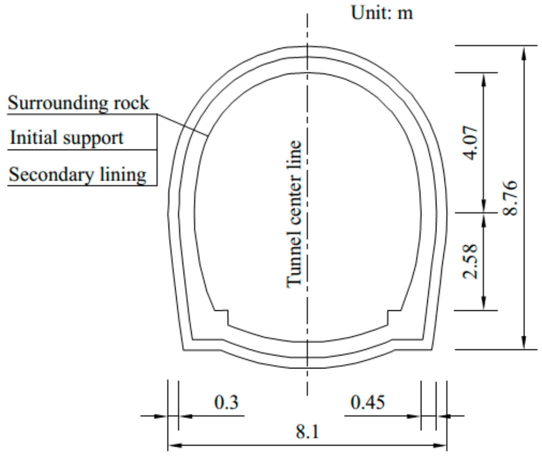

Figure 7. Tunnel dimensions.

Midas GTS NX finite element calculation software established the Load-structure model. The central line of the second lining is taken as the contour line of the model, and the contour line is a five center circle. The calculation load mainly considers the surrounding rock pressure, water pressure, structural self-weight and formation elastic resistance. The elastic resistance of formation is simulated by radial spring. The lining water pressure is calculated by the reduction coefficient method. The surrounding rock load calculation method is shown in the Code for Design of Railway tunnel [23]. After calculation, the lining load is shown in Table 8, in which the actual water pressure shall be reduced according to the working conditions. The surrounding rock load distribution and the calculation model are shown in Figure 8. The earth pressure at the bottom of the tunnel is simulated by the foundation reaction provided by the foundation spring (see Figure 8 outside the tunnel).

Table 8. The load calculation.

Vertical Earth Pressure (kPa)	Lateral Earth Pressure (kPa)	Full Head Hydrostatic Pressure (kPa)
198.7	59.6	534.0

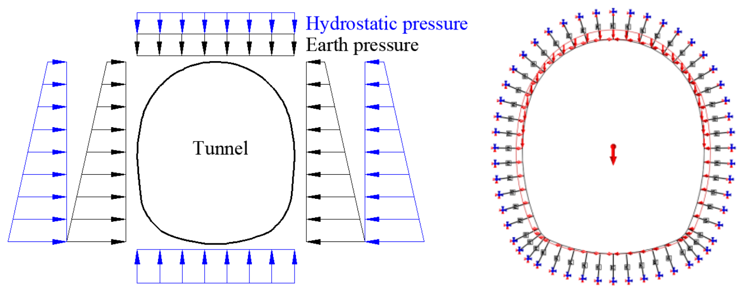

Figure 8. The calculation model.

When the water pressure reduction coefficient is 0, 0.1, 0.2, 0.4, 0.6, 0.8, and 1.0, respectively, the variation of axial force and bending moment at each part with the water pressure reduction coefficient is shown in Figures 9 and 10.

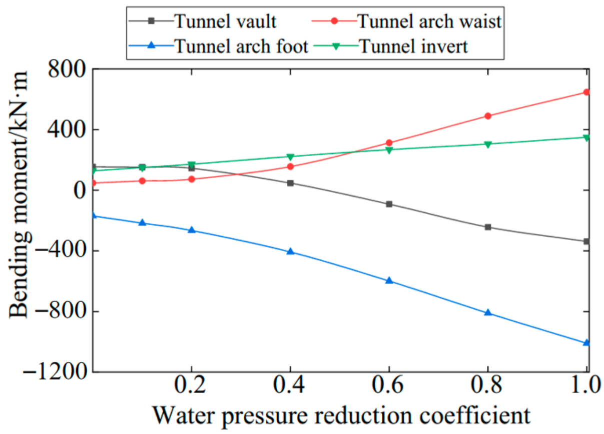

Figure 9. The relationship between bending moment and water pressure reduction coefficient.

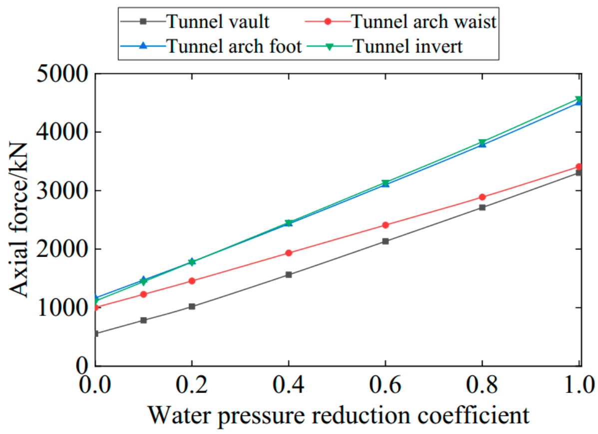

Figure 10. The relationship between axial force and water pressure reduction coefficient.

As shown in Figure 9, the bending moment of all parts except the vault increases with the increase of the water pressure reduction coefficient. Among them, the growth rate of the arch foot and arch waist increases gradually, and the growth rate of the inverted arch decreases gradually. With the increase of reduction coefficient, the lining structure at the vault is transformed from inner tension to outer tension, and then the bending moment increases gradually. When the reduction coefficient increases from 0 to 1, the bending moment at the vault changes from 154.4 kN·m to −338.2 kN·m. The arch waist increased from 47.7 kN·m to 646.8 kN·m, increasing 12.6 times. The arch foot increased from −169.5 kN·m to −1009.9 kN·m, increasing about 5 times. The inverted arch increased from 128.3 kN·m to 349.3 kN·m, increasing 1.7 times. It can be seen that the change of reduction coefficient has the greatest impact on the bending moment at the arch waist, followed by the arch foot. Under the same reduction coefficient, the bending moment at the arch foot may be significantly greater than that at other parts.

As shown from Figure 10, with the increase of the reduction coefficient, the axial force at each part increases linearly. Among them, the growth rate of the arch crown, arch foot and inverted arch is high, and the growth rate of the arch waist is lower than the others. The axial force at the vault increases from 555.1 kN to 3305.0 kN when the reduction coefficient increases from 0 to 1. The arch waist increased from 1002.2 kN to 3409.8 kN, increasing 2.4 times. The axial force value of the arch foot and the inverted arch is almost the same, increasing from about 1140 kN to about 4500 kN, an increase of nearly three times. Under the same reduction coefficient, the axial force at the arch foot and the inverted arch is larger, the axial force at the arch crown is the smallest, and the axial force distribution is positively correlated with the depth.

According to the relevant design documents of the tunnel, the existing reinforcement scheme of the lining is symmetrical reinforcement, and the strength grade of the main reinforcement is HRB400, which is generally based on Φ25@150 mm configuration, the arch foot is arranged according to 2 × Φ25@150 mm + Φ25@150 mm configuration. The structural safety factor calculation method refers to the Code for Design of Concrete Structures [28]. The safety factor of the tunnel structure is calculated based on the above reinforcement scheme, combined with the environment and purpose of the tunnel, and the specification stipulates that the safety factor of the tunnel structure shall be not less than 2.0. The calculation results of the safety factor of the lining structure are shown in Figure 11. The safety factor is defined in the Chinese tunnel design code [23]. It is mainly controlled by the axial force and a bending moment of the structure, which belongs to the category of the concrete structure. The tunnel lining is safe when the calculated safety factor is greater than 2.0.

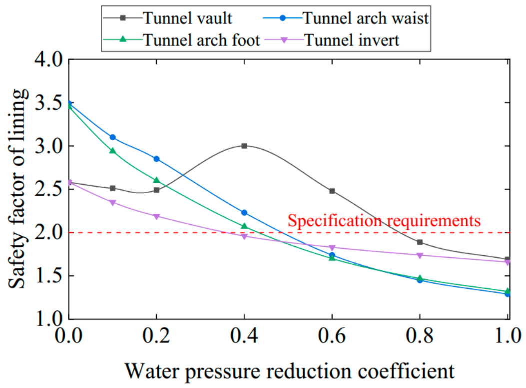

Figure 11. The safety factor varies with the reduction coefficient of water pressure.

It can be seen from Figure 11 that under the existing reinforcement scheme, with the increase of reduction coefficient, except for the temporary increase at the vault, the safety coefficient at other parts gradually decreases, and the decline rate gradually decreases. The overall safety of the lining is controlled from the inverted arch to the arch waist. Although the internal force of the arch foot is significantly greater than that of other parts, due to the strengthening of this part, the overall safety is not controlled by the arch foot. When the reduction factor is less than 0.4, the existing scheme can meet the structural safety factor's requirement to be greater than 2. The reduction coefficient increases from 0 to 1, and the safety factor at the vault decreases from 2.58 to 1.69. The safety factor at the arch waist is reduced from 3.49 to 1.29, the safety factor at the arch foot is reduced from 3.45 to 1.32, the safety factor at the inverted arch is reduced from 2.58 to 1.66, and the overall safety factor of the lining is reduced from 2.58 to 1.29. It can be seen that if the selected water reduction coefficient is smaller than the value that should be selected, the safety coefficient of the lining may be higher than the actual situation, which is contrary to safety.

3. Engineering Application

In order to verify the rationality of the lining water pressure reduction coefficient proposed in this paper and clarify the safety state of the sub-sea tunnel lining structure, the contact pressure between the initial support and the secondary lining and the internal force of the circumferential main reinforcement of the secondary lining were tracked and monitored at the construction site of the sub-sea tunnel in the Daqing section of Qingdao Metro Line 8. The secondary lining is designed by the water pressure reduction method recommended in this paper, and the design procedure is shown in Figure 12. The layout of the monitoring section and measuring points is the same as the external water pressure field test on the lining above.

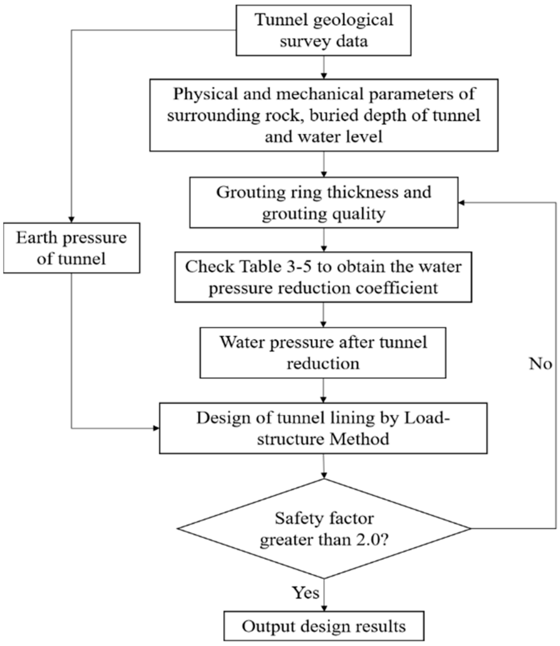

Figure 12. The design procedure of tunnel lining by water pressure reduction coefficient method.

3.1. Contact Pressure between Initial Support and Secondary Lining

The vibrating wire pressure box is used to measure contact pressure between the primary support and the secondary lining. The instrument and on-site installation photos are shown in Figure 13. After long-term tracking measurement, the contact pressure time-history curves of the primary support and secondary lining of ZDK41+943, ZDK42+092, and ZDK42+330 sections are obtained, as shown in Figure 14.

(**a**) (**b**)

Figure 13. Field installation of contact pressure sensor: (**a**) earth pressure cell; (**b**) instrument installation.

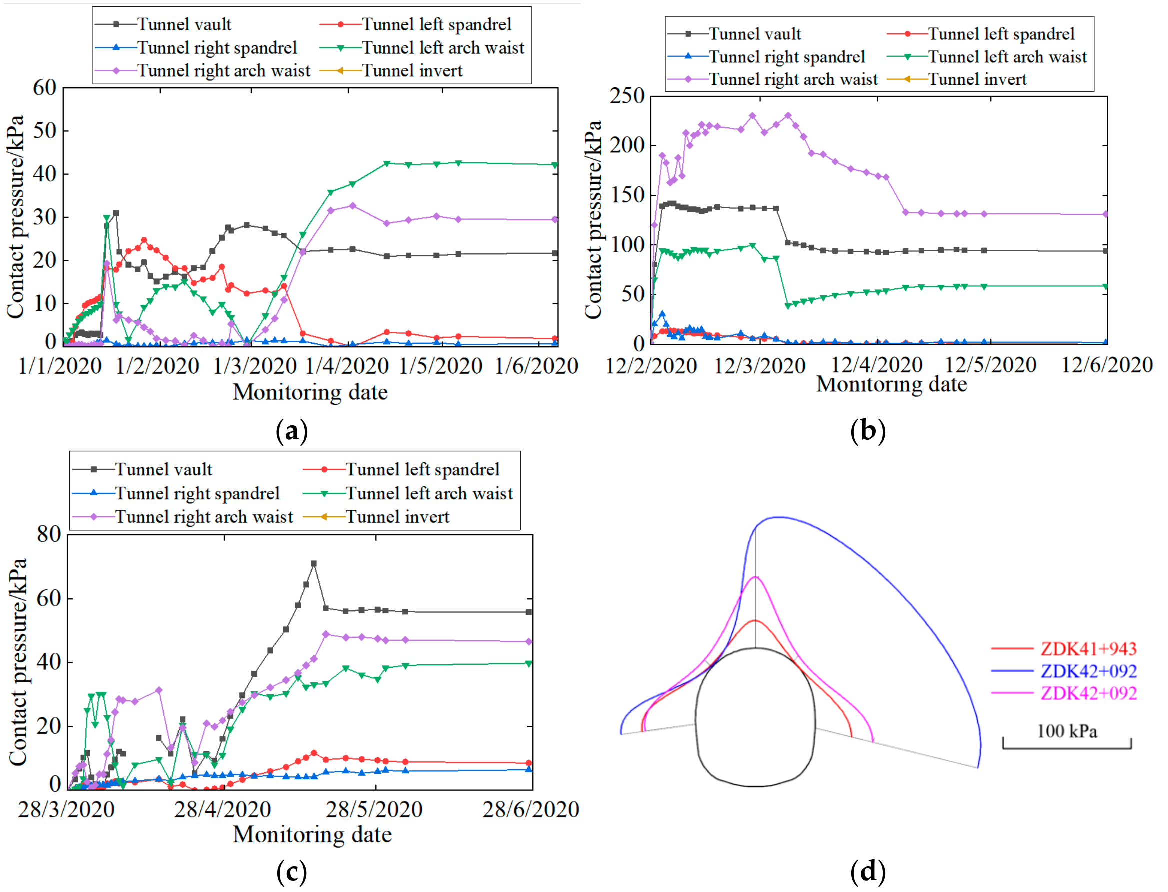

Figure 14. The contact pressure between surrounding rock and initial support: (**a**) the time-history curve of the contact pressure of the monitoring section ZDK41+943; (**b**) the time-history curve of the contact pressure of the monitoring section ZDK42+092; (**c**) the time-history curve of the contact pressure of the monitoring section ZDK42+330; (**d**) the contact pressure distribution along the section.

ZDK41+943 and ZDK42+330 sections are in class IV surrounding rock sections. After the second lining construction is completed, it does not bear excessive load immediately, the early contact pressure of each part of the lining is small, and the contact pressure at this stage shows great fluctuation. After reaching stability, the contact pressure at the arch crown and waist is large, basically 30–50 kPa, and the contact pressure at the arch shoulder is very small, all below 10 kPa. ZDK 42+092 section is located in class V surrounding rock section. Within a few days after constructing the secondary lining, the secondary lining bears a large load. Similarly, due to the influence of construction, it shows great fluctuation in the early stage and reaches a stable state after 1–2 months. After the contact pressure is stable, the maximum value appears in the right arch waist, reaching 131 kPa, followed by the arch crown and left arch waist, 94.1 kPa and 58.8 kPa, respectively.

Through comparison, it is found that the secondary lining of grade IV surrounding rock section bears a small load and reaches stability after a long rising period. The secondary lining of the grade V surrounding rock section bears a large load, which rises very fast. It can be seen that in the class IV surrounding rock section, the initial support can play a better supporting role. The load is gradually transferred to the secondary lining with its slow deformation. It is worth noting that the secondary lining load obtained from field monitoring is less than the calculated value in the specification. Therefore, it is conservative to obtain the secondary lining load through the specification.

Compared with the calculated surrounding rock load in Table 8, the on-site monitoring value of surrounding rock pressure shows that the surrounding rock load of surrounding rock IV is small, the vault is only about 28% of the calculated value of surrounding rock load, and the left arch waist is the closest, accounting for about 78%. The surrounding rock load of class V surrounding rock is large, about 48% at the vault and about 219% at the waist of the right arch. The calculation assumptions of surrounding rock load are ideal conditions, but the surrounding rock does not meet the ideal assumptions of the theory. Therefore, there is a deviation between the calculated value of surrounding rock pressure and the measured value. On the other hand, the embedding method, location and quality of monitoring instruments may affect the measured value of surrounding rock pressure.

3.2. Stress of Circumferential Main Reinforcement of Secondary Lining

The vibrating wire reinforcement stress meter is used for the stress measurement of circumferential main reinforcement of secondary lining. The instrument and on-site installation photos are shown in Figure 15. After long-term tracking measurement, the stress curves of secondary lining reinforcement at sections ZDK41+943, ZDK42+092, and ZDK42+330 are obtained, as shown in Figures 16–19.

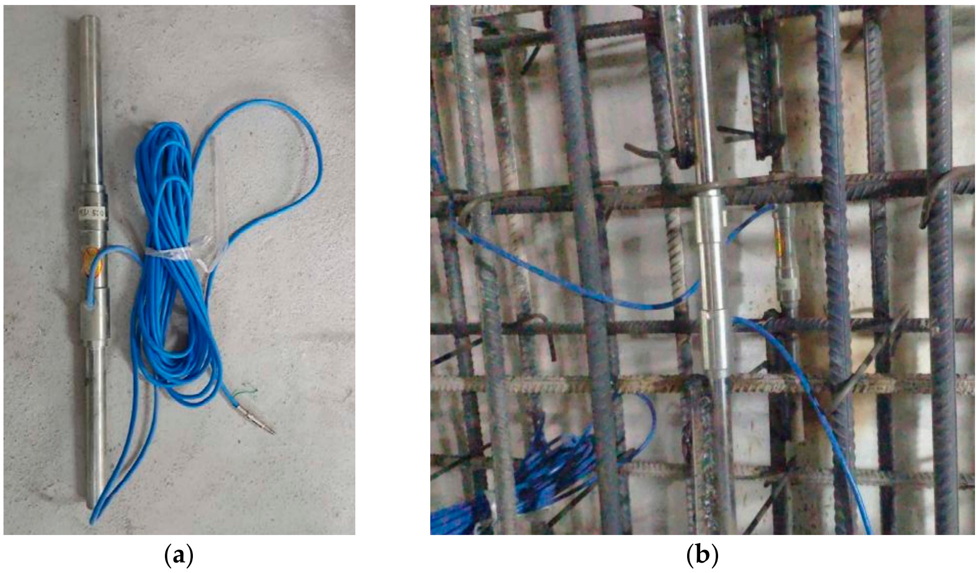

Figure 15. Field installation of reinforcement stress sensor: (**a**) reinforcement stress sensor; (**b**) instrument installation.

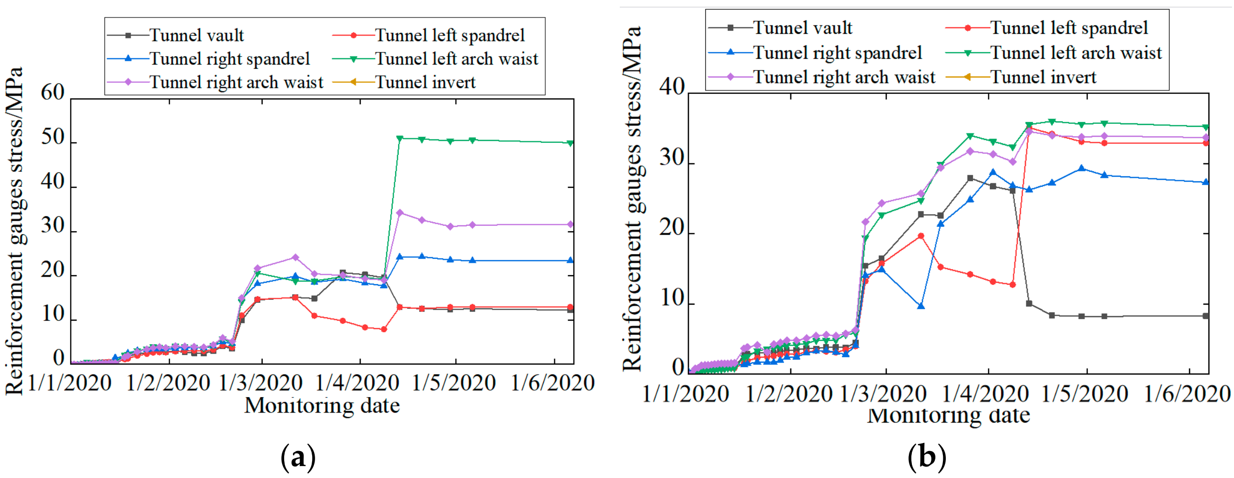

Figure 16. The time-history curve of reinforcement stress in the ZDK41+943 section: (**a**) reinforcement meter near the initial support side; (**b**) reinforcement meter away from the initial support side.

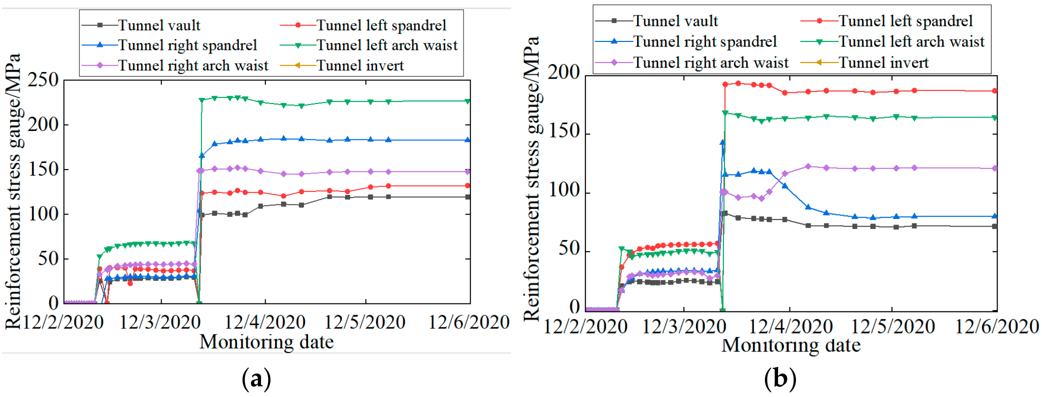

Figure 17. The time-history curve of reinforcement stress in the ZDK42+092 section: (**a**) reinforcement meter near the initial support side; (**b**) reinforcement meter away from the initial support side.

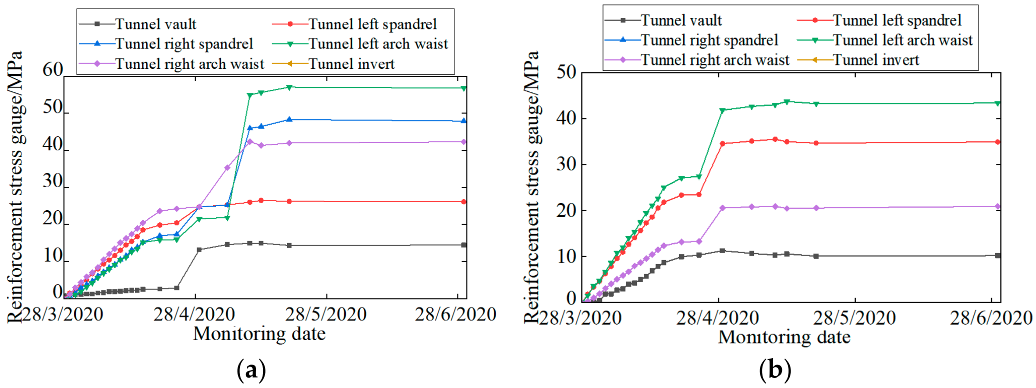

Figure 18. The time-history curve of reinforcement stress in the ZDK42+330 section: (**a**) reinforcement meter near the initial support side; (**b**) reinforcement meter away from the initial support side.

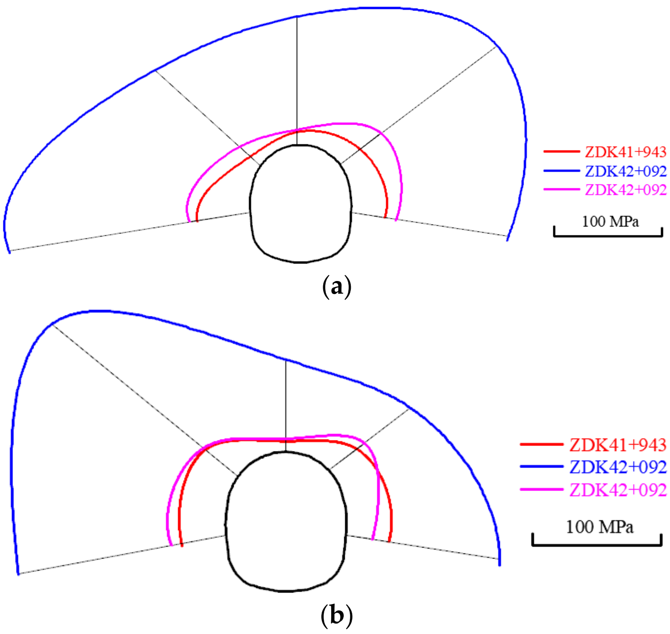

Figure 19. The reinforcement stress along the section: (**a**) reinforcement meter near the initial support side; (**b**) reinforcement meter away from the initial support side.

The curve shape of ZDK41+943 and ZDK42+330 sections of grade IV surrounding rock section is relatively similar. Among them, the stress of secondary lining reinforcement of the ZDK41+943 section is only about 5 MPa for a long time. Then, after a period of rising volatility, it gradually reached stability. The stress time history curve of secondary lining reinforcement at section ZDK42+330 changes evenly. After the two-section curves are stable, the reinforcement stress at the spandrel and waist is large, basically 30–60 MPa. The reinforcement stress at the vault is small, lower than 15 MPa. The section curve of ZDK42+092 of grade V surrounding rock section shows a stepped rise, stable after two rises. After the curve is stable, the stress value of the arch shoulder and arch waist is large, and the arch crown is small.

The maximum stress of the reinforcement near the initial support side is at the left arch waist. The maximum value of the reinforcement meter on the side away from the initial support appears at the left spandrel, 227 MPa and 187 MPa, respectively. The stress of secondary lining reinforcement is consistent with the contact stress law. The secondary lining reinforcement in grade IV surrounding rock section only bears the internal force less than 60 MPa, far from reaching the yield stress of 400 MPa, and has a relatively slow rising period. The secondary lining reinforcement in grade V surrounding rock section has large stress, the maximum value reaches 227 MPa, and the stress value increases very fast. The field test of lining structure stress found that the stratum conditions greatly impact the stress of the lining structure. The stress of secondary lining in class V surrounding the rock section is much greater than in class IV. However, there is still a large strength reserve after the stress of secondary lining reaches stability. Because the axial force and bending moment are similar to that of plain concrete when the Load-structure method is used for secondary lining design, the stress of reinforcement is not studied. In this section, the stress monitoring of reinforcement mainly illustrates the safety of secondary lining reinforcement and verifies the rationality of the water pressure reduction coefficient by comparing the difference between the actual stress of reinforcement and its yield strength.

4. Discussion

Due to the underwater environment, the sub-sea tunnel's initial support and secondary lining may bear a certain water pressure. However, determining the water pressure has always been a problem for researchers [29–31]. When the outer layer of the tunnel structure is permeable, the tunnel structure bears hydrostatic pressure. Many studies show that the water pressure borne by sub-sea tunnels is not hydrostatic pressure and is far less than hydrostatic pressure [32,33]. Practice shows that if the total hydrostatic pressure were loading the tunnels, the lining of many sub-sea tunnels, such as Seikan Tunnel [34], would have been damaged due to excessive stress. In fact, the lining is not damaged. In this way, the water pressure is reduced due to a grouting layer outside the tunnel structure and relatively complete surrounding rock. Therefore, combined with the Qingdao sub-sea tunnel, this paper studies the reduction phenomenon of lining water pressure and puts forward the corresponding reduction coefficient of tunnel lining water pressure for reference. It is worth noting that the proposed pressure reduction coefficients in Tables 4–6 can be used for a horseshoe tunnel only, and with the values that were previously defined for the thickness and permeability of the tunnel support and the water height above the tunnel. Future research can then expand the simulations for other tunnel sections (circular, for instance).

5. Conclusions

In this paper, through the numerical calculation of seepage field in sub-sea tunnels and combined with the field monitoring data, the external water pressure and its reduction coefficient of tunnel structure are studied, and the following conclusions are obtained:

(1) The height of the water level and the permeability coefficient of the surrounding rock have significant effects on the external water pressure of the initial support, but the height of the water level has little effect on the reduction coefficient of water pressure. When selecting the route of sub-sea tunnels, the buried depth of the tunnels shall be

minimized, and the unfavorable geological layer shall be avoided as far as possible under the condition of meeting the minimum overburden thickness.

(2) With the increase of initial support thickness, the initial support external water pressure and its reduction coefficient may gradually increase, but the effect is small. The decrease of the initial support permeability coefficient may lead to a significant increase of initial support external water pressure and its reduction coefficient. When the water inflow in the initial support is within a reasonable range, the permeability coefficient of the initial support can be appropriately increased, and the water pressure behind it can be reduced.

(3) The parameters of the grouting circle have a significant effect on the external water pressure and its reduction coefficient. However, after the grouting reaches a certain degree, the improvement effect of surrounding rock anti-seepage may no longer be obvious. Reasonable grouting circle parameters shall be selected for tunnel grouting, and attention shall be paid to the construction quality of the grouting circle.

(4) With the increase of water pressure, the axial force of the key sections of the tunnel increases approximately linearly, and the bending moment of each section increases; Based on the research objects defined in this paper (such as horseshoe section, water level, grouting ring), the reduction coefficient is between 0.4 and 0.6, and the tensile area of the vault is transformed from the inner side to the outer side.

(5) With the increase of water pressure reduction coefficient, the overall safety factor of lining decreases continuously; based on the research objects defined in this paper (such as horseshoe section, water level, grouting ring), when the water pressure reduction coefficient is less than 0.4, the existing scheme can meet the structural safety requirements. Therefore, the water pressure reduction coefficient has to be selected according to the ground properties, mainly permeability, and the grout properties, as defined in Tables 5–7. Moreover, the water level and the support properties may have some influence.

(6) The field test monitoring data of lining structure stress show that the stratum conditions greatly impact the stress of lining structure. The secondary lining of the grade IV surrounding rock section bears a small load, and the secondary lining of the grade V surrounding rock section bears a large load. However, there is still a large strength reserve even in the latter case.

(7) The method of designing tunnel lining based on the water pressure reduction coefficient proposed in this paper is more in line with the actual engineering situation, reduces the project's investment, and decreases the unreasonable strengthening of the lining.

Author Contributions: Conceptualization, J.Z.; methodology, Z.T.; writing—review and editing, J.Z. and N.M.; funding acquisition, Z.T. All authors have read and agreed to the published version of the manuscript.

Funding: This research was funded by the National Natural Science Foundation of China, grant number 51978041.

Institutional Review Board Statement: The participant's personal identification information used in the study did not include personal information. Ethical review and approval were not required for the study.

Informed Consent Statement: Not applicable.

Data Availability Statement: Data sharing is not applicable.

Acknowledgments: The authors would like to thank the anonymous Reviewers, the Academic Editor, and the Assistant Editor for their valuable comments that helped improve the paper's quality.

Conflicts of Interest: The authors declare no conflict of interest.

References

1. Hong, K. Typical Underwater Tunnels in the Mainland of China and Related Tunneling Technologies. *Engineering* **2017**, *3*, 871–879. [CrossRef]
2. Guo, X.; He, P.; Zhu, K.; Zhang, X.; Wang, M.; Zhu, Y. Model test research of similar materials for underwater tunnel lining in fluid-solid two-phase field. *Chin. J. Rock Mech. Eng.* **2016**, *35*, 3774–3784.
3. Zhu, C.; Ying, H.; Gong, X.; Shen, H.; Wang, X. Analytical Solutions for Seepage Field of Underwater Tunnel. In *Proceedings of China-Europe Conference on Geotechnical Engineering*; Springer Series in Geomechanics and Geoengineering; Wu, W., Yu, H.S., Eds.; Springer: Cham, Switzerland, 2018.
4. Qin, Z.; Wang, Y.; Song, Y.; Dong, Q. The Analysis on Seepage Field of Grouted and Shotcrete Lined Underwater Tunnel. *Math. Probl. Eng.* **2020**, *2020*, 7319054. [CrossRef]
5. Nilsen, B. Characteristics of Water Ingress in Norwegian Sub-sea Tunnels. *Rock Mech. Rock Eng.* **2014**, *47*, 933–945. [CrossRef]
6. Tang, X.-W.; Gan, P.-L.; Liu, W.; Zhao, Y. Surface settlements induced by tunneling in permeable strata: A case history of Shenzhen Metro. *J. Zhejiang Univ.-Sci. A* **2017**, *18*, 757–775. [CrossRef]
7. Lee, I.-M.; Nam, S.-W. The study of seepage forces acting on the tunnel lining and tunnel face in shallow tunnels. *Tunn. Undergr. Space Technol.* **2001**, *16*, 31–40. [CrossRef]
8. Lee, S.-W.; Jung, J.-W.; Nam, S.-W.; Lee, I.-M. The influence of seepage forces on ground reaction curve of circular opening. *Tunn. Undergr. Space Technol.* **2007**, *22*, 28–38. [CrossRef]
9. Nam, S.-W.; Bobet, A. Radial Deformations Induced by Groundwater Flow on Deep Circular Tunnels. *Rock Mech. Rock Eng.* **2007**, *40*, 23–39. [CrossRef]
10. Arjnoi, P.; Jeong, J.-H.; Kim, C.-Y.; Park, K.-H. Effect of drainage conditions on porewater pressure distributions and lining stresses in drained tunnels. *Tunn. Undergr. Space Technol.* **2009**, *24*, 376–389. [CrossRef]
11. Cao, Y.; Jiang, J.; Xie, K.-H.; Huang, W.-M. Analytical solutions for nonlinear consolidation of soft soil around a shield tunnel with idealized sealing linings. *Comput. Geotech.* **2014**, *61*, 144–152. [CrossRef]
12. Shin, J.H.; Addenbrooke, T.I.; Potts, D.M. A numerical study of the effect of groundwater movement on long-term tunnel behaviour. *Geotechnique* **2002**, *52*, 391–403. [CrossRef]
13. Shin, Y.-J.; Song, K.-I.; Lee, I.-M.; Cho, G.-C. Interaction between tunnel supports and ground convergence–Consideration of seepage forces. *Int. J. Rock Mech. Min. Sci.* **2011**, *48*, 394–405. [CrossRef]
14. Bouvard, M.; Pinto, N. Aménagement Caprivari-Cahoeira étude en charge. *La Houille Blanche* **1969**, *55*, 747–760. [CrossRef]
15. Fernandez, G.; Alvarez, T.A. Seepage-induced effective stresses and water pressures around pressure tunnels. *J. Geotech. Eng. ASCE* **1994**, *120*, 108–128. [CrossRef]
16. Lei, S. An Analytical Solution for Steady Flow into a Tunnel. *Ground Water* **1999**, *37*, 23. [CrossRef]
17. Harr, M.E. *Groundwater and Seepage*; McGraw-Hill Book Company: Chelmsford, Malaysia, 1962; pp. 23–25.
18. Joo, E.J.; Shin, J.H. Relationship between water pressure and inflow rate in underwater tunnels and buried pipes. *Géotechnique* **2014**, *64*, 226–231. [CrossRef]
19. El Tani, M. Circular tunnel in a semi-infinite aquifer. *Tunn. Undergr. Space Technol.* **2003**, *18*, 49–55. [CrossRef]
20. Kolymbas, D.; Wagner, P. Groundwater ingress to tunnels—The exact analytical solution. *Tunn. Undergr. Space Technol.* **2007**, *22*, 23–27. [CrossRef]
21. Huangfu, M.; Wang, M.-S.; Tan, Z.-S.; Wang, X.-Y. Analytical solutions for steady seepage into an underwater circular tunnel. *Tunn. Undergr. Space Technol.* **2010**, *25*, 391–396. [CrossRef]
22. Wang, X.; Tan, Z.; Wang, M. Theoretical and experimental study of external water pressure on tunnel lining in controlled drainage under high water level. *Tunn. Undergr. Space Technol.* **2008**, *23*, 552–560. [CrossRef]
23. Professional Standards Compilation Group of People's Republic of China. *Code for Design of Railway Tunnel (TB10003-2016)*; China Communications Press: Beijing, China, 2016.
24. Li, Z. Study on Sulphate Corrosion Characteristics and Life Evaluation of Tunnel Sprayed Shotcrete. Master's Thesis, Chang'an University, Chang'an, China, 2019.
25. Wang, J.; Niu, D.; He, H.; Wang, B. Durability degradation of lining shotcrete exposed to compound salt. *China Civ. Eng. J.* **2019**, *52*, 79–90.
26. Liu, H. Causes of defects in tunnel concrete shotcrete and treatment suggestions. *Build. Technol. Dev.* **2018**, *45*, 100–101.
27. Professional Standards Compilation Group of People's Republic of China. *Code for Design of Metro (GB 50157-2013)*; China Communications Press: Beijing, China, 2013.
28. Professional Standards Compilation Group of People's Republic of China. *Code for Design of Concrete Structures (GB 50010-2010)*; China Communications Press: Beijing, China, 2010.
29. Zhang, Y.; Zhang, D.; Fang, Q. Analytical solutions of non-Darcy seepage of grouted sub-sea tunnels. *Tunn. Undergr. Space Technol.* **2020**, *96*, 103182. [CrossRef]
30. Li, S.-C.; Liu, H.-L.; Li, L.-P. Large scale three-dimensional seepage analysis model test and numerical simulation research on undersea tunnel. *Appl. Ocean. Res.* **2016**, *59*, 510–520. [CrossRef]
31. Li, X.-B.; Zhang, W.; Li, D.-Y.; Wang, Q.-S. Influence of underground water seepage flow on surrounding rock deformation of multi-arch tunnel. *J. Cent. South Univ. Technol.* **2008**, *15*, 69–74. [CrossRef]

32. Li, X.-F.; Du, S.-J.; Chen, B. Unified analytical solution for deep circular tunnel with consideration of seepage pressure, grouting and lining. *J. Cent. South Univ.* **2017**, *24*, 1483–1493. [CrossRef]
33. Fotieva, N.N.; Sammal, A.S. Calculation of pressure tunnel linings with consideration of consolidation grouting of the rocks. *Hydrotech. Constr.* **1987**, *21*, 6–8. [CrossRef]
34. Tuchiya, Y.; Kurakawa, T.; Matsunaga, T.; Kudo, T. Research on the Long-Term Behaviour and Evaluation of Lining Concrete of the Seikan Tunnel. *Soils Found.* **2009**, *49*, 969–980. [CrossRef]